Impact of tropical cyclones on the ocean heat budget in the Bay of Bengal during 1999: 1. Model configuration and evaluation

Jih-Wang Wang,[1] Weiqing Han,[1] and Ryan L. Sriver[2]

Received 18 July 2012; accepted 8 August 2012; published 18 September 2012.

[1] The impacts of two consecutive, strong tropical cyclones (TCs) – 04B (10/15–10/19) and 05B (10/25–11/3) in 1999 (hereafter, TC1 and TC2) – on the upper ocean temperature and surface height of the Bay of Bengal (BoB) are examined using the Hybrid Coordinate Ocean Model (HYCOM). The HYCOM control run is driven by the Cross-Calibrated MultiPlatform (CCMP) satellite winds, European Center for Medium-Range Weather Forecasts Re-analysis Interim (ERAI) surface reanalysis data, and Tropical Rainfall Measuring Mission precipitation. In order to investigate ocean response to high wind conditions, which are not well resolved by the CCMP or ERAI products, a modified Rankine vortex is adopted to reconstruct the TC winds in an experimental run. Wind stress is determined from wind speed when considering the level-off and decline of drag coefficient at wind speed of 34 m/s and greater. The experimental run reproduces the strong SST reduction ($\sim -3^{\circ}$C) near the Orissa seashore along and on the right of the TC tracks. TC2 (category 5) cools the BoB SST less than TC1 (category 4) likely due to the initial SST depression by TC1. TC2 has higher winds and lingers over the ocean longer than TC1, and hence the onshore Ekman transport and mass convergence induced by TC2 wind is more prominent. The HYCOM mixed layer temperatures and depths to the south of the BoB generally agree with the observations very well. The simulations, however, have weaker vertical temperature gradient in the thermocline layer, suggesting that HYCOM produces a more diffusive thermocline than the observations.

Citation: Wang, J.-W., W. Han, and R. L. Sriver (2012), Impact of tropical cyclones on the ocean heat budget in the Bay of Bengal during 1999: 1. Model configuration and evaluation, *J. Geophys. Res.*, *117*, C09020, doi:10.1029/2012JC008372.

1. Introduction

1.1. Background

[2] Quantifying oceanic meridional heat transport has important implications for climate research. The equator-to-pole transport of heat by the ocean-atmosphere system buffers temperature extremes, allowing the climate system to reach radiative equilibrium and thus regulating climate. Using an inverse approach, *Macdonald and Wunsch* [1996] estimated that the world's oceans transport roughly half of the heat that moves from the tropics to the poles, while the atmosphere carries the other half. Moreover, the ocean is considered the primary contributor in the tropics [e.g., *Held*, 2001]. The ocean's capability to store and transport heat may also be linked to the sequestration of the global warming signal [*Meehl et al.*, 2005, 2011]. The ocean heat transport (OHT) from the tropics to the poles consists of three major components: a) downward diapycnal heat transfer into the ocean in the tropics, b) poleward OHT into the high latitudes, and c) heat release back to the atmosphere. Estimating meridional OHT, however, remains challenging, and significant discrepancies exist among different estimates [e.g., *Gordon et al.*, 2000; *Trenberth and Caron*, 2001; *Held*, 2001]. In addition, observed diapycnal diffusivities in the lower latitudes are typically too low to account for the required downward heat flux inferred from budget analyses [e.g., *Ledwell et al.*, 1993; *Gregg et al.*, 2003]. The measurements of Ledwell *et al.* and Gregg *et al.* were primarily made under low wind conditions, because it is very difficult to avoid the interference of turbulence under high wind conditions. Consequently, diapycnal turbulent mixing induced by strong winds, such as those associated with tropical cyclones (TCs), has been shown to be an important mechanism for vertical ocean mixing budgets in the tropics [*Sriver and Huber*, 2007; *Sriver et al.*, 2008] and it has been hypothesized these events may contribute substantially to global OHT [*Emanuel*, 2001].

[1]Department of Atmospheric and Oceanic Sciences, University of Colorado Boulder, Boulder, Colorado, USA.
[2]Department of Atmospheric Sciences, University of Illinois at Urbana-Champaign, Urbana, Illinois, USA.

Corresponding author: J.-W. Wang, Department of Atmospheric and Oceanic Sciences, University of Colorado Boulder, 311 UCB, Boulder, CO 80309, USA. (jihwang@colorado.edu)

0148-0227/12/2012JC008372

1.1.1. Tropical Cyclone (TC) Impacts on Ocean Heat Pumping and Heat Transport

[3] *Price* [1981] showed that the cyclonic rotation of the wind field associated with moving TCs causes near-inertial oscillations in the wake, which increases shear instability at the bottom of the mixed layer (ML) and induces strong upper ocean mixing. Because the tropical oceans are stably stratified, vertical mixing leads to upwelling of cold water and a reduction in sea surface temperature (SST). *Black* [1983] suggested that cold water entrainment at the bottom of the ML may account for over 80% of the observed SST decreases in the wake of a TC. *Emanuel* [2001] hypothesized that the turbulent mixing induced by TCs' winds could homogenize the upper ocean temperature, thus lowering SST, warming the upper thermocline, and potentially causing a net oceanic heat convergence through restoration of cold anomalies via enhanced surface fluxes and advection. This net oceanic heat convergence, or downward ocean heat pumping (DOHP), measures the amount of heat that is pumped down into the thermocline by the TC winds-induced turbulent mixing process. In steady state, this additional heat would be later carried away from storm-affected regions by lateral advection and has been hypothesized to be important for the ocean's heat budget and transport. *Emanuel* [2001] used a simple coupled ocean-hurricane model to estimate the net ocean heating induced by global TC activities during 1996. He concluded that the TC-related heating is approximately 1.4 ± 0.7 PW (1 PW = 10^{15}W), which may account for a substantial portion of the OHT carried by the meridional overturning circulation.

[4] As more in situ and satellite observations become available, advancements have been made to improve our understanding of hurricane- and typhoon-induced upper ocean variability in the Atlantic and Pacific Oceans through both observational and modeling studies [e.g., *Jacob and Shay*, 2003; *Black et al.*, 2007; *D'Asaro et al.*, 2007; *Yin et al.*, 2007; *Siswanto et al.*, 2008; *Huang et al.*, 2009; *Lin et al.*, 2009; *Wada et al.*, 2009; *Jiang et al.*, 2009; *Tseng et al.*, 2010; *Zheng et al.*, 2010]. In an effort to improve the estimate of TC impacts on upper ocean heat budget, *Jacob and Shay* [2003] produced improved forcing fields by blending field observations for Hurricane Gilbert of 1988 with reanalysis data, and then used the forcing fields to drive an oceanic general circulation model (OGCM). *Sriver and Huber* [2007] used the observed SST before and after TCs to calculate the global heat exchange due to TCs, based on the hypothesis of *Emanuel* [2001]. Their estimate suggests that TCs contribute ~0.26 PW to OHT, which is considerably smaller than the *Emanuel*'s [2001] original 1.4 ± 0.7 PW estimate. Furthermore, *Sriver et al.* [2008] showed that adopting seasonally and spatially varying upper ocean temperature profiles and using different SST products can result in ~60% change in DOHP estimates. The discrepancies among different estimates demonstrate the need for an improved understanding and quantification of how and why the upper ocean heat content (OHC) is altered and redistributed by TCs.

1.1.2. Impacts of TCs in the Indian Ocean

[5] Compared to the Pacific and Atlantic Oceans, fewer studies of TC-induced upper ocean variability have been done in the Indian Ocean. *Gopala Krishna et al.* [1993] showed the oceanic thermal response to a severe cyclonic storm in May, 1999 and recognized the importance of upper ocean mixing and upwelling in determining the subsequent air-sea heat exchange. *Murty et al.* [1996] provided a good background hydrographic description of the Bay of Bengal (BoB) and discussed the effect of a deep depression in August, 1990 on the upper ocean heat content. Attention also has been paid to the devastating societal and economical impacts of the TCs, such as the very severe TC Nargis in May 2008 [e.g., *Fritz et al.*, 2009]. In the BoB, cyclones are often active during spring (pre-monsoon season) and fall (post-monsoon season). By analyzing satellite and in situ observations, existing studies have documented the ocean-atmosphere conditions and their co-variability associated with TC Nargis [e.g., *Shi and Wang*, 2008; *Kikuchi et al.*, 2009; *Yu and McPhaden*, 2011]. It has been shown that SST dropped by over 2–3°C, wave heights were 3–4 m to the right of the cyclone, and oceanic biological activity and suspended matter apparently increased after Nargis' passage, indicating that Nargis caused strong oceanic mixing.

[6] In this paper, we focus on two Indian Ocean TCs in 1999 that landed at Orissa, India: 04B (hereafter TC1) and 05B (hereafter TC2). A few studies have investigated the influence of SST on the intensity and track of TC2, and vice versa. It is suggested that better-resolved SST spatial and temporal variations may improve TC2 intensity and track prediction in the model [*Mandal et al.*, 2007; *Bongirwar et al.*, 2011], and the region of maximum surface cooling shifted to the left of the cyclone track when the TC translated over the coastal waters [*Mahapatra et al.*, 2007]. *Chinthalu et al.* [2001] showed vigorous temperature and salinity anomalies induced by TC2, and *Subrahmanyam et al.* [2005] described the history of TC1 and TC2 and attempted a regression relationship between the outgoing longwave radiation and ocean surface response. To date, studies on TCs' effects on DOHP and OHT in the BoB have not yet been done. How does the upper ocean respond to TCs in the BoB, and how is the response compared with similar events in Atlantic and Pacific Oceans? Due to the large amount of freshwater input from monsoon rainfall and river runoff into the BoB, the upper ocean is strongly stratified and the barrier layer persists [e.g., *Han et al.*, 2001; *Howden and Murtugudde*, 2001; *Masson et al.*, 2002; *Vinayachandran et al.*, 2002]; for barrier layer definition see *Lukas and Lindstrom* [1991] and *Sprintall and Tomczak* [1992]. *Sengupta et al.* [2008] suggested that post-monsoon TCs have lesser effect on SST cooling as revealed by satellite observations, likely because freshwater input from river runoff and monsoon rainfall leads to temperature inversion, where warmer water resides below the surface and forms a barrier layer. Mixing due to strong TC winds entrains warmer water into the surface layer, and thus produces less cooling.

1.2. Present Research About the TC Effects on the BoB Heat Budget

[7] The BoB is geographically unique in that it is a semi-enclosed basin, which is bounded by continents to the north, east and west but is open to the warm Indian Ocean SST in the south. As a result, this region is subject to strong forcing from the seasonally reversing monsoon winds and precipitation. The strong rainfall associated with the summer monsoon,

together with a large amount of freshwater discharged from the Ganges-Brahmaputra, Irrawaddy, and other smaller rivers into the Bay, make the BoB one of the freshest parts of the world's oceans. This seasonal freshening increases the stratification and limits vertical mixing. On the other hand, strong monsoon and TC winds may overcome the strong stratification and mix heat downward. Due to its semi-enclosed nature, excessive heat accumulated in the BoB has to be transported southward out of the Bay.

[8] The goal of this study is to understand how the upper ocean in the BoB responded to the two TCs that landed at Orissa in 1999, with special emphasis on the upper ocean heat budget, including DOHP and OHT. The research is presented in two parts. Part 1 focuses on model configuration and evaluation, while part 2 [*Wang et al.*, 2012] assesses the processes by which the two TCs cause the upper ocean heat change. The rest of part 1 is organized as follows. Section 2 describes the two TC cases, the configuration of the OGCM – the Hybrid Coordinate Ocean Model (HYCOM) that is used for ocean response simulations, the surface forcing fields and experiment design. TC winds reconstruction and the wind stress calculation are also described in section 2. Section 3 reports our results on the comparison between the model simulations and observations, and section 4 provides a summary and conclusions.

2. Description of Cyclone Cases, Ocean Model and Experiments

2.1. Description of the TCs

[9] In this study, we choose two consecutive TC cases – 04B (10/15 00Z – 10/19 06Z) and 05B (10/25 00Z – 11/3 06Z) – that occurred in 1999. Cyclone 04B (TC1) formed over the center of the BoB on 10/15 and traveled west-northwestward across the BoB. After explosive intensification on 10/16, TC1 was classified as category 4 at 10/17 00Z and turned northward before it made landfall on the same day at Orissa, India (see Figure 1, top left, for its track and bottom left for the maximum sustainable wind speed).

[10] Within a week after TC1 dissipated, a tropical depression crossed the Malay Peninsula on 10/25 and then intensified into a cyclone on 10/27 while it traveled northwestward. Cyclone 05B (TC2) reached category-5 strength at 10/28 18Z and made landfall to the northeast of the landfall location of TC1 after a rapid intensification (Figure 1, top right and bottom right). It stalled inland and weakened to a tropical storm. The tropical storm turned southward and re-entered the BoB on 10/30 and turned in a south-southwestward direction. TC2, also known as the 1999 Orissa cyclone, was one of the deadliest TCs in the century and resulted in more than 10,000 casualties [*International Federation of Red Cross and Red Crescent Societies*, 2001]. The cyclone winds reached ~72 m/s (~140 knots) with an estimated minimum central pressure of lower than 912 hPa before it hit Orissa, India. The rainfall over southeast India caused record flooding in the low-lying areas [*U.S. Navy*, 1999] partly due to the soil saturated by TC1 rainfall and the topographical stalling of TC2 over land. The total effect of storm surge, tide and local topography on sea level elevation at Paradip, Orissa was reported to be 5–6 m [*Latha and Rama Rao*, 2007]. The occurrence of these two intense TCs during a short time span offers a unique opportunity to examine how surface heat fluxes and ocean heat transport within the BoB were modified by their passage.

2.2. The HYbrid Coordinate Ocean Model (HYCOM) and Forcing Fields

[11] HYCOM utilizes terrain-following sigma coordinates in coastal regions, isopycnic coordinates in the open ocean interior, and z coordinates in very shallow waters and near the surface. The details of the model dynamics and physics are documented in *Bleck* [2002] and *Halliwell* [1998, 2004]. HYCOM has been applied in a wide range of studies with various timescales and regions, including the Indian Ocean [*Han*, 2005; *Han et al.*, 2006a, 2006b; *Yuan et al.*, 2006; *Han et al.*, 2007; *Han and Webster*, 2002], the Atlantic Ocean [*Han et al.*, 2008], the Black Sea [*Kara et al.*, 2005a, 2005b], the tropical Pacific Ocean [*Shaji et al.*, 2005], and the Gulf of Mexico [*Prasad and Hogan*, 2007].

2.2.1. Indian Ocean Configuration

[12] In this paper, the model is configured to the Indian Ocean (35°S–30°N, 20°E–120°E) with a horizontal resolution of 0.25° × 0.25°. This resolution is eddy permitting and can reasonably resolve the impacts of TC forcings on the upper ocean, given that the radii of 18 m/s (~35-kt) winds in TC1 and TC2 sometimes exceeded 220 km (~120 nautical miles) and the radii of 51 m/s (~100-kt) wind (if any) were always at least 28 km (~15 nautical miles), as shown in U.S. NRL (Naval Research Laboratory) TC warnings. Vertically, 30 hybrid layers are chosen with fine resolution in the upper ocean to better resolve the vertical structures of upper ocean currents, temperature, and salinity. The first layer is set to be 3 m deep, and the thickness of the following layers increases as an exponent of 1.125 (i.e., layer n thickness $H_n = 3 \times 1.125^n$) until the coordinate transforms to sigma coordinate. With the choice of the aforementioned hybrid coordinates and sigma values, the number of layers for the top 50 m ranges from three layers near Burma's coast to 10 layers in the southwest corner of the BoB. Realistic bottom topography from the National Geophysical Data Center (NGDC) 2′ × 2′ digital bathymetry is used with 2° × 2° smoothing.

[13] A reference pressure of sea level is adopted, because we focus on upper ocean processes. Nonlocal K-profile parameterization (KPP) is used for the boundary layer mixing scheme [*Large et al.*, 1994, 1997]. Background diffusivity for internal wave mixing is set to 5×10^{-6} m^2/s [*Gregg et al.*, 2003], and viscosity is set to be an order of magnitude larger (5×10^{-5} m2/s; *Large et al.*, 1994]. The diapycnal mixing coefficient is 1×10^{-7} m^2 s^{-2}/N, where N is the buoyancy frequency. Isopycnal momentum dissipation values are formulated as $u_d x$, where x is the local horizontal mesh size and u_d is set to be 0.015 ms^{-1} for Laplacian dissipation and 0.005 m/s for biharmonic dissipation. A similar method is used for temperature and salinity diffusion, with $u_d = 0.001$ m/s for Laplacian diffusion. Near the southern boundary and the Indonesian Throughflow region, sponge layers of five degrees are applied to relax the model temperature and salinity to the monthly ocean objective analysis product from the Meteorology Office of the UK [*Ingleby and Huddleston*, 2007].

2.2.2. Surface and Lateral Boundary Forcing Fields

[14] The HYCOM surface forcing fields include 2 m air temperature, 2 m humidity, surface net solar radiative flux

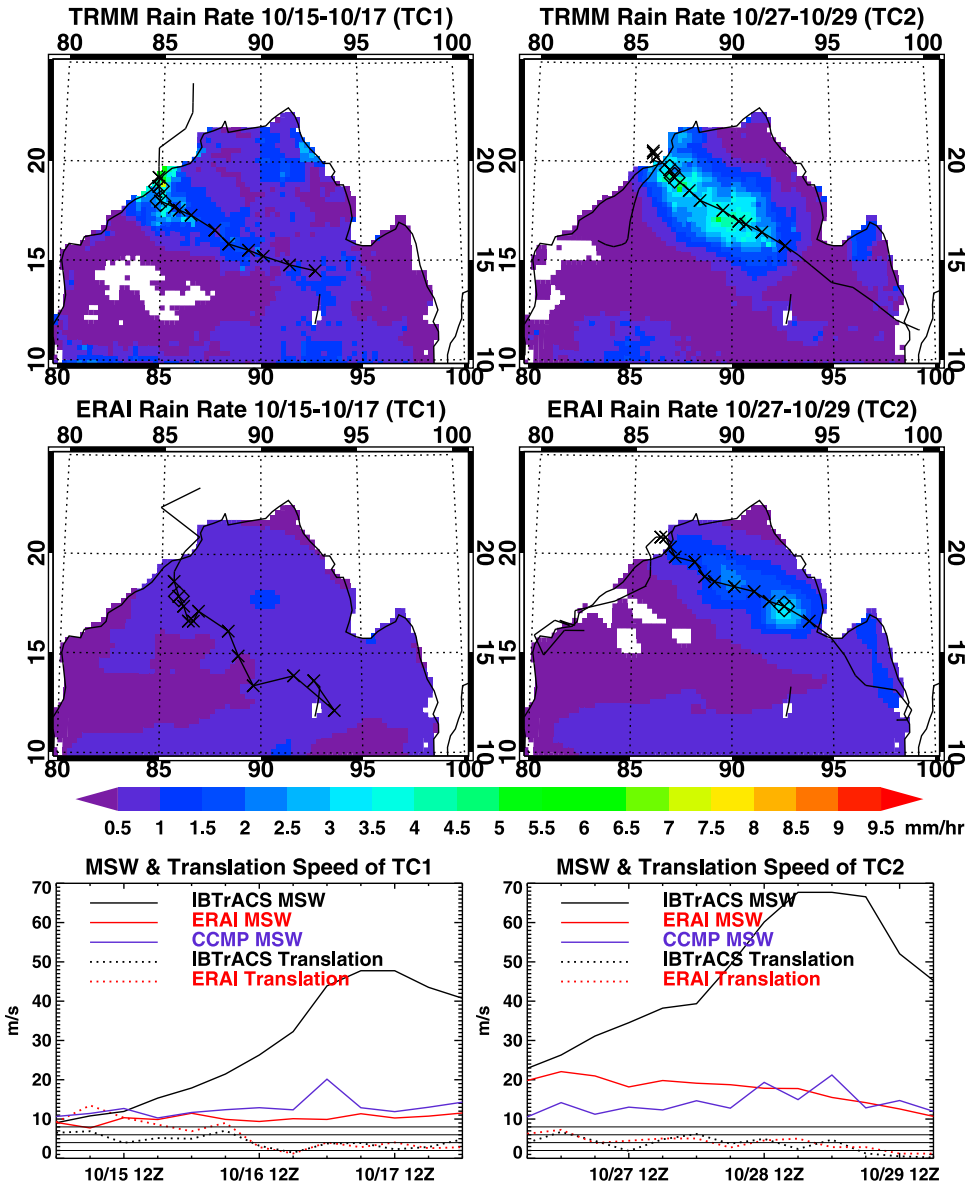

Figure 1. (top) The three-day mean TRMM 3B42 rain rate, (middle) the three-day mean ERAI rain rate, and (bottom) maximum sustainable wind speed (MSW) and translation speed (bottom panels) for the two TC cases. For TC1, the rain rate averaging period is 10/15–10/17, while for TC2, 10/27–10/29. The black lines are the cyclone tracks from IBTrACs (top panels) and determined from ERAI lowest mean sea level pressure (middle panels), while the crosses are the cyclone centers every six hours during the three-day period. Missing values and zero precipitation in TRMM data are shown as white background. Note that TC1 center from ERAI at 10/15 00Z is ambiguous.

and net radiative flux (shortwave plus longwave), precipitation, wind speed and wind stress. The sea surface latent and sensible heat fluxes are determined by HYCOM SST, wind speed, air temperature and specific humidity, following the Coupled Ocean-Atmosphere Response Experiment (COARE 3.0) algorithm [*Fairall et al.*, 2003]. This algorithm allows medium to strong wind conditions with a wind speed of ~40 m/s. Both reanalysis products and satellite observations are used to force HYCOM, as discussed below.

2.2.2.1. The ERA-Interim (ERAI) Fields

[15] The 6-hourly ECMWF (European Centre for Medium-Range Weather Forecasts) Re-analysis Interim (ERAI) products [*Simmons et al.*, 2007; *Dee et al.*, 2011] for the period of 1989–2008 are used to force HYCOM. The ERAI data assimilation uses 12-h 4D-Var at T255 horizontal resolution (~0.7031252°). The 6-hourly surface analysis fields, including 2 m air temperature, 2 m humidity, 10 m wind velocity, and 6-hourly surface accumulated fields, including wind stress, precipitation, surface net longwave radiation, and surface net solar radiation, are extracted for HYCOM forcing fields. All fields are interpolated onto HYCOM grids. The ERAI sea level pressure fields are also used to track the TC center positions. The center positions from ERAI differ by up to 2° central angle compared to International Best Track

Table 1. The Largest Three Rivers in the Model Domain Based on *Dai et al.* [2009]

River Name	Annual Flow Volume (Sv)	Observation Start	Observation End
Brahmaputra	2.179×10^{-2}	1956/01	2000/12
Ganges	1.273×10^{-2}	1949/01	1996/12
Irrawaddy	1.240×10^{-2}	1978/01	1988/12

Archive for Climate Stewardship (IBTrACS) data during the strengthening stage (Figure 1, top and middle).

2.2.2.2. TRMM Precipitation

[16] The Tropical Rainfall Measuring Mission (TRMM) [*Kummerow et al.*, 1998, 2000] MultiSatellite Precipitation Analysis (TMPA) intercalibrates and combines TRMM 2A-12, SSMI, AMSR and AMSU precipitation estimates from different orbiting satellites, referred to as high quality estimates. Rain rate estimates by the geostationary satellites' infrared band observations are then also made by fitting the infrared brightness temperatures to the high quality estimates. The infrared rain rate estimates have 3-hourly or higher temporal resolution. Both the rain rates are scaled to match the monthly satellite/rain gauge analyses. The TRMM 3B42 product (0.25° × 0.25°, 3-hourly and 50°S–50°N) is used to force HYCOM. Its retrieval algorithm can be found in *Huffman et al.* [1995, 2007] and *Huffman* [1997]. For HYCOM experiments, the 3-hourly product is integrated onto a 6-hourly interval to be consistent with other forcing fields.

[17] TRMM precipitation data provide stronger rainfall estimates and more accurate TC locations than the ERAI precipitation data (Figure 1). The TRMM rain rate averaged over the time frame of the two TC cases and superimposed on their tracks from IBTrACS, which is endorsed by The World Meteorological Organization Tropical Cyclone Program (data from http://www.ncdc.noaa.gov/oa/ibtracs/), is shown in Figure 1 (top). The rainy area during 10/15–10/17 covers most of the BoB, and its strongest rate happens after the explosive intensification of TC1 (10/17). For TC2, the strong rainy area is more concentrated along its track.

2.2.2.3. CCMP Wind

[18] The global (78.375°S to 78.375°N) 6-hourly Cross-Calibrated MultiPlatform (CCMP) ocean surface winds on 0.25° × 0.25° grids [*Atlas et al.*, 2008, 2009] are also used to force HYCOM (see section 2.3). The CCMP winds are derived from cross-calibrating ocean surface wind data from SSM/I, TMI, AMSR-E, SeaWinds on QuikSCAT, and SeaWinds on ADEOS-II. These data sets are combined with conventional observations and ECMWF wind field (as a starting/background estimate of wind field), by using a variational analysis method. The CCMP winds more accurately depict the TCs' locations than the ERAI winds (not shown). Although CCMP TC wind speeds are not always higher than ERAI in our cases, the former is more accurate in the timing of strongest stage than the latter (Figure 1, bottom).

[19] *Powell et al.* [2003] and *Oey et al.* [2007] showed that the drag coefficient (C_{10}) increases with the increase of 10 m wind speed (V) up to about 34 m/s [also see *Large and Pond*, 1981], but then levels off and declines at even stronger wind speeds. In this study, wind stress (τ_x and τ_y) is determined from V and air density (ρ) by the formula suggested by *Sanford et al.* [2007] and *Zedler* [2009]:

$$10^3 C_{10} = \begin{cases} 1.2 & \mathrm{V} < 11\ \mathrm{m/s} \\ [1.21.72.01.81.5] & \mathrm{V} = [11\ \ 28\ \ 34\ \ 40\ \ 50]\mathrm{m/s}, \\ 1.5 & \mathrm{V} > 50\ \mathrm{m/s} \end{cases} \tag{1}$$

$$\tau_x = \rho C_{10} V u, \tag{2}$$

$$\tau_y = \rho C_{10} V v.$$

[20] The drag coefficient for wind speed between 11, 28, 34, 40, and 50 m/s is linearly interpolated accordingly.

2.2.2.4. Lateral Boundary Forcing: Bay of Bengal River Discharge

[21] The three largest rivers that run into the BoB are the Brahmaputra, Ganges, and Irrawaddy (Table 1). Instead of relaxing the salinity in the northern BoB toward climatological values [e.g., *Duncan and Han*, 2009], we utilize the monthly river discharge data from *Dai et al.* [2009] as freshwater input to force HYCOM. The discharge data are based on the gauge records at the farthest downstream stations for the world's 925 largest ocean-reaching rivers, and the data gaps in the records are filled through linear regression between the observed streamflow and the streamflow simulated by Community Land Model version 3. For the Brahmaputra and Ganges, the discharge data are better covered by the gauge records for the period of our HYCOM simulations, while for the Irrawaddy, the discharge data for the same period are all from model simulation results (see Table 1 for observation coverage time frame).

2.3. Reconstructed TC Winds

[22] Quantitatively, neither the CCMP nor ERAI winds are able to represent the observed TCs' maximum sustainable wind speeds (Figure 1, bottom), although the general cyclonic circulation patterns are captured. The winds from both CCMP and ERAI are too weak, even though sometimes CCMP winds show better agreement with the IBTrACS data (Figure 1). This is because TC's high winds are generally associated with strong precipitation, which contaminates satellite wind retrieval under high wind conditions. Although efforts are being made to tackle this problem, the issue exists for the best available CCMP winds. The underestimation of wind speed may underestimate the mixing and heat pumping effects of the TCs.

[23] In order to investigate oceanic response to high wind conditions (≥18 m/s), a modified Rankine vortex [*Holland*, 1980] is adopted for azimuthal wind velocity:

$$V = \begin{cases} \dfrac{V_{\max}}{R} \times r & , \text{for } r < R \\ V_{\max} \times \left(\dfrac{R}{r}\right)^x & , \text{for } r \geq R \end{cases}. \tag{3}$$

[24] $V_{\max}$ is the maximum sustainable azimuthal wind speed of the TC, and R is the radius of maximum sustainable wind (MSW). The radial profile of wind is proportional to r

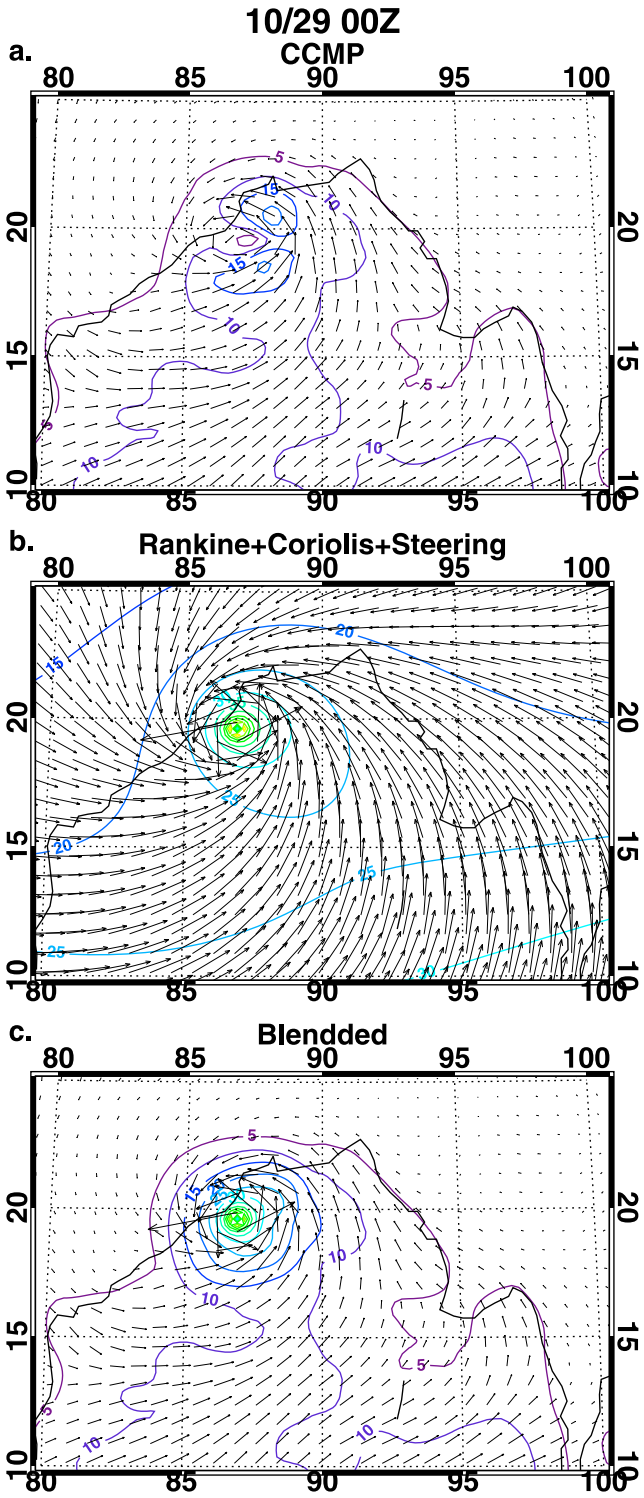

Figure 2. Wind speed (contours; 5 m/s interval) and wind velocity (arrows) for the products from (a) CCMP, (b) modified Rankine vortex plus Coriolis effect and translation velocity, and (c) the blended product. The blended wind (Figure 2c) is made of Figures 2a and 2b.

within R and to $1/r^x$ beyond R. The parameter x is estimated to range from 0.4 to 0.6 [*Holland*, 1980], and 0.5 is used for this research. To account for the Coriolis effect, we further adjust V so that the absolute angular momentum ($rV + fr^2/2$) is conserved at the same r, where the Coriolis parameter f changes with latitudes. The radial velocity is assumed to be $-0.3V$ [*Zedler et al.*, 2002] within R and decrease at 1/12 of the rate of decrease of the tangential wind speed outside R, similar to Hurricane Eloise in *Price* [1981].

[25] An example of implementation of modified Rankine vortex, considering the Coriolis effect and translation velocity and its blending with the CCMP wind field at 10/29 00Z, when TC2 wind speed peaked, is shown in Figures 2b and 2c. Linear ramping has been applied in space for the blending to ensure the smooth transition from the centers of the TCs to two times of 35-kt radii of the TCs. Note that to conserve absolute angular momentum, the modified Rankine vortices have the greatest wind speed in the lower latitudes, and only half of the storm translation velocity is added to the modified Rankine vortices, as recommended by *NOAA* [1979].

2.4. Experiments

[26] HYCOM is first spun up for 20 years using the 1989–2008 monthly climatologies of ERAI forcing fields (section 2.2.2.1). Restarting from the spin-up solution, HYCOM is integrated forward in time for the period of 1989–2000 using the 6-hourly CCMP winds (section 2.2.2.3), and 6-hourly ERAI data for other forcing fields. The 6-hourly (integrated from original 3-hourly data) TRMM 3B42 precipitation (section 2.2.2.2) replaces the ERAI precipitation to drive the model starting in 1998. This run is driven by the original forcing fields, and is referred to as Main Run (MR). The model results for 1989–1991 are not analyzed, because they contain transient features that result from the transition of the spin-up (monthly climatological driving forces) to the simulation driven by the 6-hourly forcing fields.

[27] One additional experimental run, referred to as RcWIND, is performed branching from the MR solution on 10/11, 1999 by forcing HYCOM with the reconstructed winds (section 2.3), because the maximum CCMP wind speed in the MR is only ~20 m/s during TC1 and TC2, which underestimates the TC effects on mixing, entrainment and advection. All the surface forcings in RcWIND are the same as in the MR, except the reconstructed wind field for TC1 and TC2. While the MR and RcWIND have the same values before 10/11, 1999, the differences between the MR and RcWIND solutions afterwards provide quantitative estimates of the strong wind effects of the TCs.

3. Model-Data Comparison

3.1. Sea Surface Temperature

[28] The SST changes during TC1 and TC2 from TRMM data show a general "Bay-wide" cooling for TC1 and cooling in the western and eastern Bay for TC2, with the maximum cooling (~−3°C) occurring at three locations for both TC1 and TC2 (Figures 3a and 3d): near the Orissa seashore along the tracks, in the southwestern BoB (10°N–15°N 80°E–85°E), and in the eastern BoB (east of 94°N). The spatial patterns of TC-associated cooling are basically simulated by RcWIND (driven by the modified Rankine vortex; Figures 3b and 3e) and the MR (driven by the CCMP winds; Figures 3c and 3f), albeit with significant differences in some regions. The well-documented rightward skew in the SST response relative to the TC track [e.g., *Price*, 1981; *Jacob et al.*, 2000] near offshore Orissa can be seen for TC1

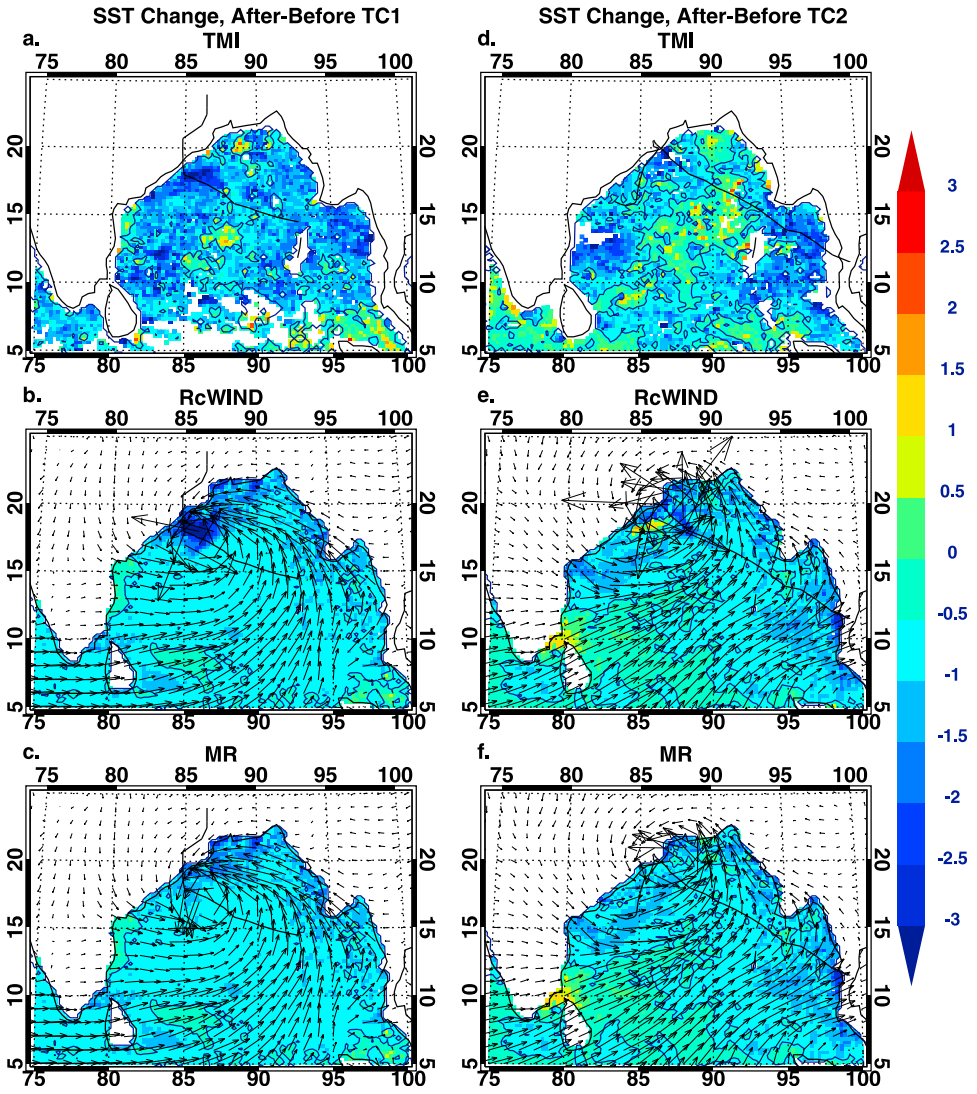

Figure 3. SST differences between 10/12–10/14 mean and 10/19–10/21 mean (TC1 effect) from (a) Tropical Rainfall Measuring Mission (TRMM) – Microwave Imager (TMI), (b) the RcWIND run, and (c) the MR and between 11/3–11/5 mean and 10/22–10/24 mean (TC2 effect) from (d) TMI, (e) RcWIND, and (f) the MR. The superimposed black lines are the tracks of TC1 (Figures 3a–3c) and TC2 (Figures 3d–3f). The winds near the strongest stage (10/17 00Z for TC1 and 10/29 00Z for TC2) of the TCs are also plotted (vectors in the middle and bottom panels). The black contour is for 0°C SST.

in the observations, the RcWIND run and MR (Figures 3a–3c). The CCMP winds that include the TCs are much weaker than the best estimates in the IBTrACS or NRL warnings, and therefore the SST decrease near Orissa is much weaker in the MR than in RcWIND, especially for TC1. Evidently, TC2 cools the SST less than TC1 (category 4), even though TC2 (category 5) is stronger (see section 2.1), which is likely due to the initial SST depression by the occurrence of TC1.

[29] Quantitatively, the simulated cooling by the MR and RcWIND is much weaker than the observed cooling in the southwestern and eastern BoB for both of the TC cases, and the weak warming in the central BoB, especially for TC2, is not shown in the model. Several possible reasons may account for the model/data differences. First, TMI measures sea skin temperature, whereas HYCOM SST is from the top slab layer (3 m thick), which may partly explain the lesser sensitivity of HYCOM solutions to the TC forcings. Second, errors in HYCOM forcing fields will cause errors in the simulated SST. For example, ERAI data may not adequately resolve the spatial variations and amplitude of the radiative fluxes, air temperature and/or specific humidity near the TC centers; the reconstructed winds, although much stronger than the CCMP winds, may not always be physically consistent with other forcing fields. Third, HYCOM's limitations may also contribute to its less sensitive SST response.

[30] Neither the MR nor RcWIND captures the strong SST reduction in the southwestern BoB. Before TC1, TMI shows relatively warm SST (≥31°C) in the southwestern BoB, in contrast to the relatively cool SST (≤28°C) in the south central BoB. TMI data suggest that the low SST in the south central BoB may originate from the minicold pool south of the India-Sri Lanka channel (not shown), which is consistent with the findings of *Rao et al.* [2006a, 2006b]. During TC1, the SST in the southwestern BoB is reduced partly by the

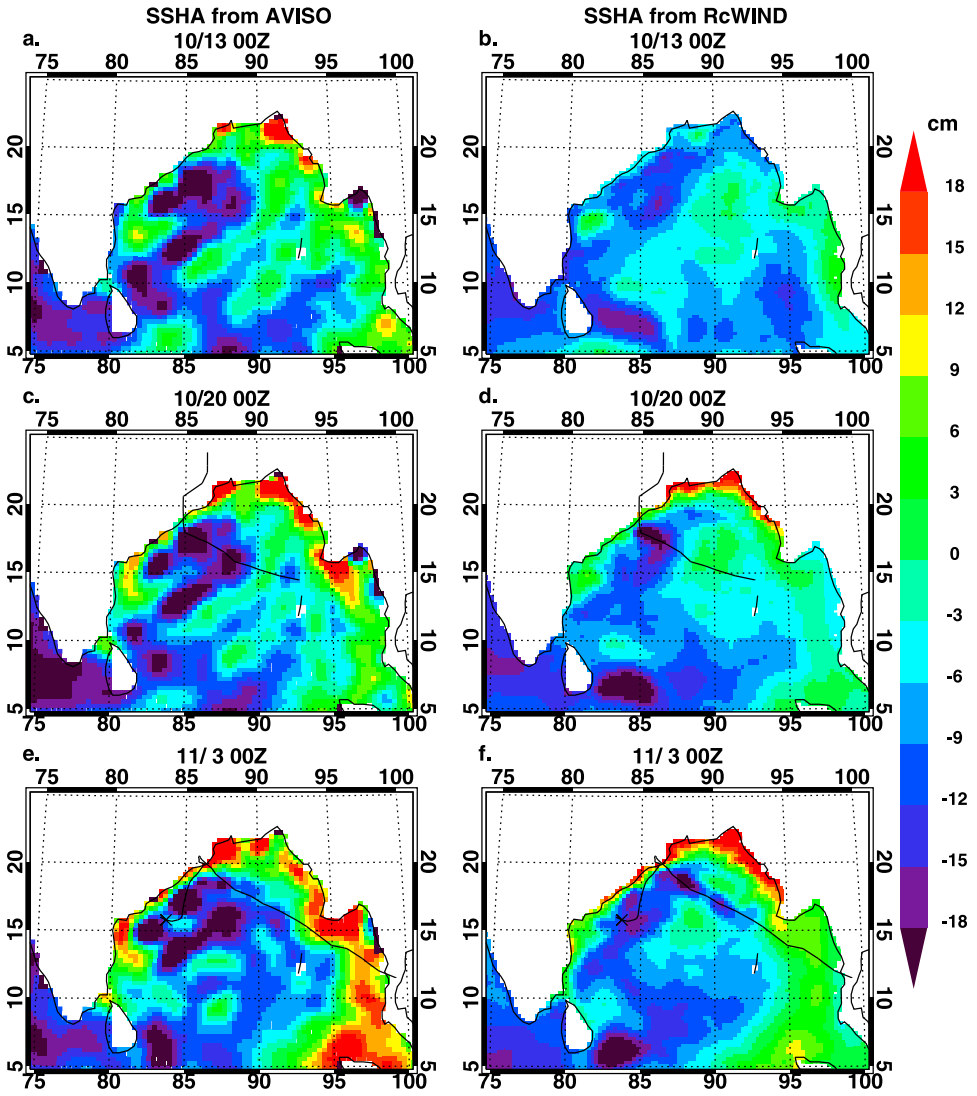

Figure 4. Sea surface height anomaly at three different times from (a, c, e) AVISO and (b, d, f) the RcWIND experiment during the TCs' period.

enhanced surface heat loss caused by the strengthened wind, and partly by the cold advection from the south central BoB. The SST contrast between the two regions is not as obvious in HYCOM as in TMI before TC1; therefore, the cold advection during TC1 is not as strong in HYCOM. The SST decrease in the southwestern BoB during TC2 is caused by a different process. TMI data show that TC2 cools SST along its track before its landfall location and along Orissa shore after it reenters the Bay by strong mixing and upwelling (see part 2 for discussions). The cold seawater is then advected to the southwestern BoB by the strong counterclockwise current along the coast. HYCOM does not capture the full strength of the SST decrease along the Orissa shore after 10/29 due to the early termination of wind reconstruction period, and therefore does not reduce SST as much in the southwestern BoB by advection as in TMI observations.

3.2. Sea Surface Height

[31] Strong winds associated with the two TCs near Andaman Islands and along the northern BoB boundary (Figure 3, middle and bottom) cause onshore Ekman transport and thus onshore mass convergence, raising the sea level near the coasts by as much as >10 cm in some regions, as shown by the AVISO satellite observed sea surface height (SSH) (Figures 4a, 4c, and 4e). This sea level signal can propagate counter-clockwise around the perimeter of the Bay, increasing the SSH along the western BoB boundary. Meanwhile, the onshore mass convergence induces mass divergence and sea level fall in the central Bay. In addition, positive Ekman pumping velocity

$$w_e = \frac{\partial}{\partial x}\left(\frac{\tau^y}{\rho f}\right) - \frac{\partial}{\partial y}\left(\frac{\tau^x}{\rho f}\right)$$

associated with the TC winds also favors Ekman divergence and thus sea level fall. The observed sea level rise along the coasts and fall in the Bay interior are reasonably simulated by the MR and RcWIND, although the simulated SSH is weaker in amplitude especially in the eastern BoB (Figures 4b, 4d, and 4f). Along the TC tracks before they arrive at Orissa,

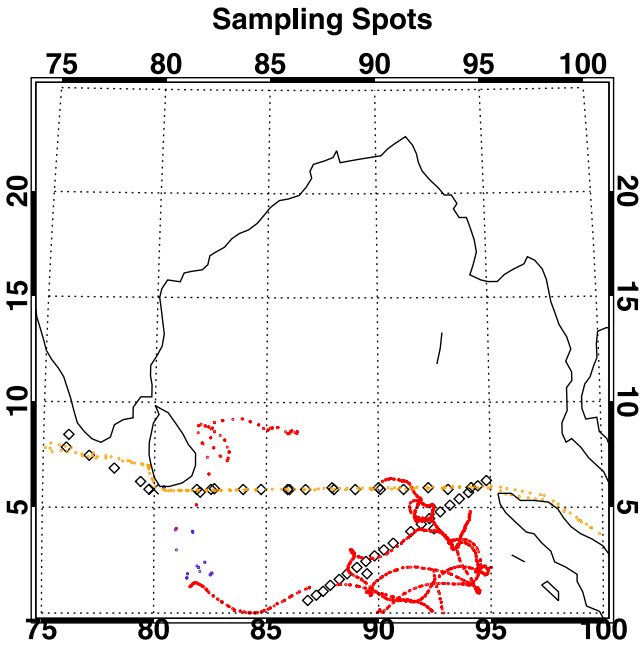

Figure 5. The buoy and cruise sampling locations from October to December, 1999. Red and blue dots represent good quality temperature data by drifting buoys, while brown dots are "unchecked" temperature data. Black diamonds represent cruise campaigns that collect not only surface but also subsurface temperature data. Blue dots are the drifting buoys measurements in the region of 80°E–82.7°E, 0°N–5°N after 11/16 in 1999. See text for more description for the purpose of separating blue from red.

both of the TCs are reaching their strongest stages. The cold SST induced by TC-associated wind near Orissa may also contribute to the sea level fall there.

[32] TC1 exhibits larger SST impacts than TC2, as we discussed in section 3.1, whereas TC2 exhibits larger SSH impacts than TC1. TC2 has higher winds and lingers over the ocean longer than TC1, and hence the onshore Ekman transport and mass convergence induced by TC2 cyclonic wind is more prominent.

3.3. Drifting Buoys and Cruise Profiles

[33] The model's skill in reproducing surface and subsurface variability is also evaluated against surface measurements using drifting buoys and surface and subsurface measurements by cruises from October to December, 1999 (Data Source: Department of Fisheries and Oceans Canada, Science Sector, Integrated Science Data Management). Since the sampling locations (Figure 5) are generally located between the equator and 10°N, the data are used to evaluate HYCOM results along the BoB southern boundary. Unfortunately, there are no in situ measurements north of 10°N from October to December, 1999. Argo floats were not yet deployed in the BoB at that time.

[34] The MR SST compare favorably with the high quality buoy observations (standard error = 0.43°C), with SST values from 27°C to 30°C (red crosses in Figure 6). The SST and subsurface temperature from RcWIND are similar to those of the MR, indicating that the reconstructed high wind speeds near the center of the TCs, which are used to drive RcWIND, do not have strong influence on upper ocean thermal structure outside the BoB. In the region of 80°E–82.7°E, 0°N–5°N during 11/16–12/31 in 1999, the MR SST (blue dots in Figure 5 and blue triangles in Figure 6) and TMI observed 3-day mean SST are both generally above 27°C, much higher than the buoy observations; by comparing with TMI SST, we are less confident in the buoy data quality for this location and time.

[35] HYCOM reasonably simulates the ML temperature and depth except for a few locations in early October 1999 (Figure 7). TC1 starts from 10/15 and ends on 10/19, while TC2 starts from 10/25 and ends on 11/3. Therefore, the profiles in Figure 7 show comparisons before, during and after the TC events. ML temperatures and depths in HYCOM generally agree with the observations very well. HYCOM simulations, however, have weaker vertical temperature gradient in the thermocline layer, suggesting that HYCOM produces a more diffusive thermocline than the observations. Indeed, as we increase the number of vertical layers from 22 to 30, the simulated thermocline is improved (not shown). The ML depth is generally shallower than or near 100 m, depending on locations and seasons, while the thermocline layer is usually between 100 m to 300 m.

4. Summary and Discussion

[36] In this paper, we document the experiment design and results of simulations using an eddy-permitting ocean general circulation model – HYCOM, examining the upper-ocean impacts in the BoB caused by two consecutive TCs during

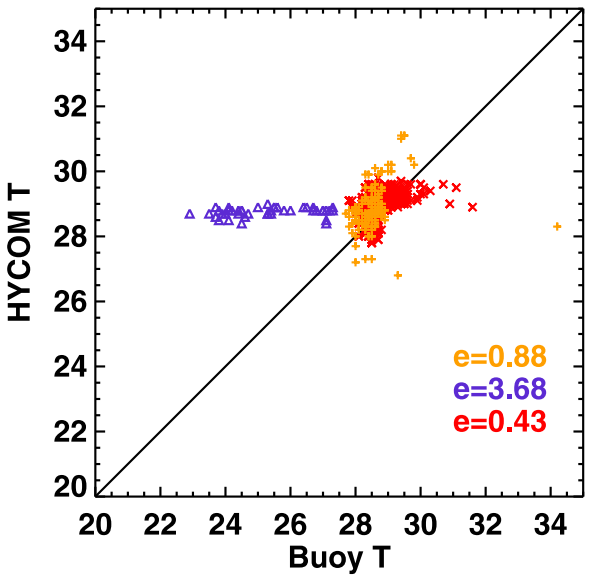

Figure 6. SST comparisons between the MR results and drifting buoy observations. Blue triangles are for the data in the region of 80°E–82.7°E, 0°N–5°N after 11/16 in 1999, red crosses are for the data when measurements have good quality and not classified as blue (see text for explanations), and brown crosses for "unchecked" measurements. The numbers shown on the lower right portion of the Figure are standard errors. The RcWIND results are very similar to those of the MR.

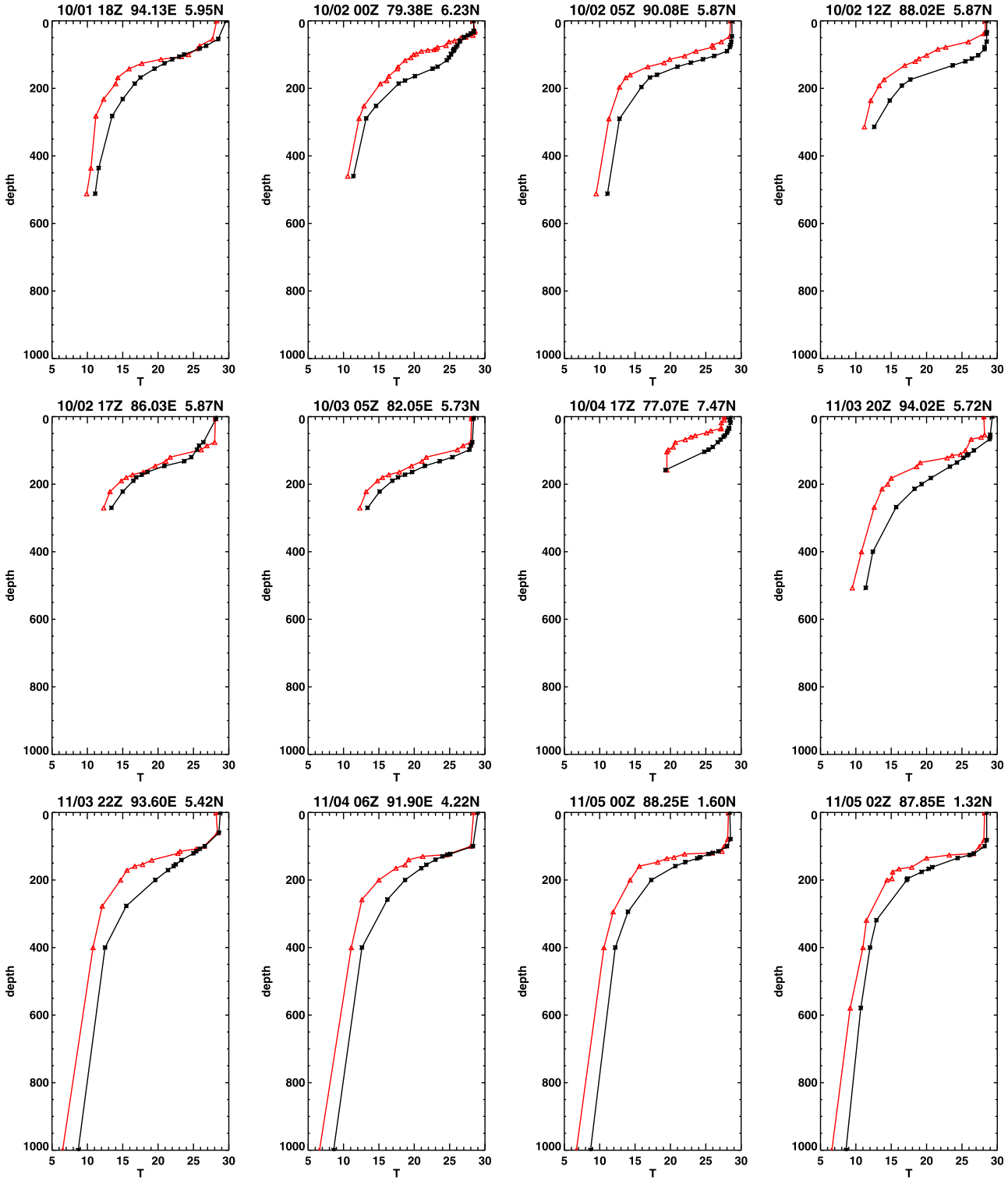

Figure 7. Temperature profiles from cruise observations (red) and from HYCOM RcWIND (black). The MR and RcWIND have almost identical temperature profiles from the equator to 10°N. Only 12 out of 47 temperature profiles are shown to demonstrate the model skill from 76°E to 96°E at every 2° interval (Figure 5, black diamonds) during October–November, 1999.

October–November 1999. The implications of these results for the BoB heat budget will be examined in the companion paper (part 2). The HYCOM simulations are designed and performed using 0.25° × 0.25° grids and 30 vertical layers, which is driven by satellite-observed CCMP winds, TRMM precipitation, and ERA-Interim reanalysis radiative flux and other forcing variables (section 2.2). Freshwater input from medium to large rivers surrounding the BoB are also included.

The above forcing fields are able to capture the observed TC1 and TC2 identified by the IBTrACS data, although the CCMP winds significantly underestimate the maximum wind speeds associated with the TCs (section 2.1 and Figure 1). To overcome this underestimation, one additional experiment is performed using reconstructed TC-wind velocities based on the modified Rankine vortex as in *Holland* [1980] (section 2 and Figure 2).

[37] Solutions from the HYCOM MR and RcWIND run with enhanced TC winds reasonably reproduce the upper ocean thermal structure and SSH in the BoB compared with cruise and satellite observations, albeit with quantitative model/data differences. HYCOM simulations, however, exhibit weaker vertical temperature gradients in the thermocline layer, suggesting a more diffusive thermocline in the model than in the observations. The strong SST reduction ($\sim -3^{\circ}$C) near the Orissa seashore along the tracks and on the right is shown in RcWIND. Compared to the TMI observations, the contrast between the high SST in the southwestern BoB and low SST in the south central BoB during TC1 is less evident in RcWIND and results in weaker cold advection from the south central BoB to the southwestern BoB. Also, RcWIND produces weaker SST reduction in the eastern and southwestern BoB during TC2, possibly due to the lack of enough information for TC wind reconstruction in the two regions. TC2 (category 5) generally cools the "Bay-wide" SST less than TC1 (category 4) likely due to the initial SST depression by TC1. On the other hand, the onshore Ekman transport and mass convergence induced by TC2 cyclonic wind is more prominent because of the stronger winds and longer lifetime than TC1 over the ocean.

[38] **Acknowledgments.** We would like to thank Luc Bujold for providing buoy and cruise observation data, Allan Wallcraft for HYCOM consultation, and anonymous reviewers for their precious comments. We also thank CISL of NCAR for providing computer resources and technical support. Jih-Wang Wang and Weiqing Han are supported by NSF CAREER award 0847605, NASA OSTST award NNX08AR62G, and NOAA NA11OAR4310100.

References

Atlas, R., J. Ardizzone, and R. N. Hoffman (2008), Application of satellite surface wind data to ocean wind analysis, *Proc. SPIE*, *7087*, 70870B, doi:10.1117/12.795371.

Atlas, R., R. N. Hoffman, J. Ardizzone, S. M. Leidner, and J. C. Jusem (2009), Development of a new cross-calibrated, multi-platform (CCMP) ocean surface wind product, paper presented at 13th Conference on Integrated Observing and Assimilation Systems for Atmosphere, Oceans, and Land Surface, Am. Meteorol. Soc., Phoenix, Ariz.

Black, P. G. (1983), Ocean temperature changes induced by tropical cyclones, PhD dissertation, 278 pp., Pa. State Univ., State College.

Black, P. G., E. A. D'Asaro, W. M. Drennan, J. R. French, P. P. Niller, T. B. Sanford, E. J. Terrill, E. J. Walsh, and J. A. Zhang (2007), Air-sea exchange in hurricanes, *Bull. Am. Meteorol. Soc.*, *88*, 357–374, doi:10.1175/BAMS-88-3-357.

Bleck, R. (2002), An oceanic general circulation model framed in hybrid isopycnic-Cartesian coordinates, *Ocean Modell.*, *4*, 55–88, doi:10.1016/S1463-5003(01)00012-9.

Bongirwar, V., V. Rakesh, C. M. Kishtawal, and P. C. Joshi (2011), Impact of satellite observed microwave SST on the simulation of tropical cyclones, *Nat. Hazards*, *58*(3), 929–944, doi:10.1007/s11069-010-9699-y.

Chinthalu, G. R., P. Seetaramayya, M. Ravindran, and P. N. Mahajan (2001), Response of the Bay of Bengal to Gopalpur and Paradip super cyclones during 15–31 October, 1999, *Curr. Sci.*, *81*(5), 283–291.

D'Asaro, E. A., T. B. Sanford, P. P. Niiler, and E. J. Terrill (2007), Cold wake of Hurricane Frances, *Geophys. Res. Lett.*, *34*, L15609, doi:10.1029/2007GL030160.

Dai, A. D., T. Qian, K. E. Trenberth, and J. D. Milliman (2009), Changes in continental freshwater discharge from 1948 to 2004, *J. Clim.*, *22*, 2773–2792, doi:10.1175/2008JCLI2592.1.

Dee, D. P., et al. (2011), The ERA-Interim reanalysis: Configuration and performance of the data assimilation system, *Q. J. R. Meteorol. Soc.*, *137*, 553–597, doi:10.1002/qj.828.

Duncan, B., and W. Han (2009), Indian Ocean intraseasonal SST variability during boreal summer: Madden-Julian Oscillation versus submonthly forcing and processes, *J. Geophys. Res.*, *114*, C05002, doi:10.1029/2008JC004958.

Emanuel, K. (2001), Contribution of tropical cyclones to meridional heat transport by the oceans, *J. Geophys. Res.*, *106*(D14), 14,771–14,781, doi:10.1029/2000JD900641.

Fairall, C. W., E. F. Bradley, J. E. Hare, A. A. Grachev, and J. B. Edson (2003), Bulk parameterization of air-sea fluxes: Updates and verification for the COARE algorithm, *J. Clim.*, *16*, 571–591, doi:10.1175/1520-0442(2003)016<0571:BPOASF>2.0.CO;2.

Fritz, H. M., C. D. Blount, S. Thwin, M. K. Thu, and N. Chan (2009), Cyclone Nargis storm surge in Myanmar, *Nat. Geosci.*, *2*(7), 448–449, doi:10.1038/ngeo558.

Gopala Krishna, V. V., V. S. N. Murty, M. S. S. Sarma, and J. S. Sastry (1993), Thermal response of upper layers of Bay of Bengal to forcing of a severe cyclonic storm: A case study, *Indian J. Mar. Sci.*, *22*, 8–11.

Gordon, C., C. Cooper, C. A. Senior, H. Banks, J. M. Gregory, T. C. Johns, J. F. B. Mitchell, and R. A. Wood (2000), The simulation of SST, sea ice extents and ocean heat transports in a version of the Hadley Centre coupled model without flux adjustments, *Clim. Dyn.*, *16*, 147–168, doi:10.1007/s003820050010.

Gregg, M. C., T. B. Sanford, and D. P. Winkel, (2003), Reduced mixing from the breaking of internal waves in equatorial waters, *Nature*, *422*, 513–515, doi:10.1038/nature01507.

Halliwell, G. R. (1998), Simulation of North Atlantic decadal/multi-decadal winter SST anomalies driven by basin-scale atmospheric circulation anomalies, *J. Phys. Oceanogr.*, *28*, 5–21, doi:10.1175/1520-0485(1998)028<0005:SONADM>2.0.CO;2.

Halliwell, G. R. (2004), Evaluation of vertical coordinate and vertical mixing algorithms in the HYbrid Coordinate Ocean Model (HYCOM), *Ocean Modell.*, *7*, 285–322, doi:10.1016/j.ocemod.2003.10.002.

Han, W. (2005), Origins and dynamics of the 90-day and 30–60 day variations in the equatorial Indian Ocean, *J. Phys. Oceanogr.*, *35*, 708–728, doi:10.1175/JPO2725.1.

Han, W., and P. J. Webster (2002), Forcing mechanisms of sea-level interannual variability in the Bay of Bengal, *J. Phys. Oceanogr.*, *32*, 216–239, doi:10.1175/1520-0485(2002)032<0216:FMOSLI>2.0.CO;2.

Han, W., J. P. McCreary, and K. E. Kohler (2001), Influence of precipitation minus evaporation and Bay of Bengal rivers on dynamics, thermodynamics, and mixed layer physics in the Indian Ocean, *J. Geophys. Res.*, *106*, 6895–6916, doi:10.1029/2000JC000403.

Han, W., G. A. Meehl, and A. Hu (2006a), Interpretation of tropical thermocline cooling in the Indian and Pacific Oceans during recent decades, *Geophys. Res. Lett.*, *33*, L23615, doi:10.1029/2006GL027982.

Han, W., T. Shinoda, L.-L. Fu, and J. P. McCreary (2006b), Impact of atmospheric intraseasonal oscillations on the Indian Ocean dipole during the 1990s, *J. Phys. Oceanogr.*, *36*, 670–690, doi:10.1175/JPO2892.1.

Han, W., D. Yuan, W. Timothy Liu, and D. J. Halkides (2007), Intraseasonal variability of Indian Ocean sea surface temperature during boreal winter: MJO versus submonthly forcing and processes, *J. Geophys. Res.*, *112*, C04001, doi:10.1029/2006JC003791.

Han, W., P. J. Webster, J. Lin, W. T. Liu, R. Fu, D. Yuan, and A. Hu (2008), Dynamics of intraseasonal sea level and thermocline variability in the equatorial Atlantic during 2002–2003, *J. Phys. Oceanogr.*, *38*, 945–967, doi:10.1175/2008JPO3854.1.

Held, I. M. (2001), The partitioning of the poleward energy transport between the tropical ocean and atmosphere, *J. Atmos. Sci.*, *58*, 943–948, doi:10.1175/1520-0469(2001)058<0943:TPOTPE>2.0.CO;2.

Holland, G. J. (1980), An analytic model of the wind and pressure profiles in hurricanes, *Mon. Weather Rev.*, *108*, 1212–1218, doi:10.1175/1520-0493(1980)108<1212:AAMOTW>2.0.CO;2.

Howden, S. D., and R. Murtugudde (2001), Effects of river inputs into the Bay of Bengal, *J. Geophys. Res.*, *106*(C9), 19,825–19,843, doi:10.1029/2000JC000656.

Huang, P. S., T. B. Sanford, and J. Imberger (2009), Heat and turbulent kinetic energy budgets for surface layer cooling induced by the passage of Hurricane Frances (2004), *J. Geophys. Res.*, *114*, C12023, doi:10.1029/2009JC005603.

Huffman, G. J. (1997), Estimates of root-mean-square random error for finite samples of estimated precipitation, *J. Appl. Meteorol.*, *36*(9), 1191–1201, doi:10.1175/1520-0450(1997)036<1191:EORMSR>2.0.CO;2.

Huffman, G. J., R. F. Adler, B. Rudolf, U. Schneider, and P. R. Keehn (1995), Global precipitation estimates based on a technique for combining satellite-based estimates, rain gauge analysis, and NWP model precipitation information, *J. Clim.*, *8*(5), 1284–1295, doi:10.1175/1520-0442(1995)008<1284:GPEBOA>2.0.CO;2.

Huffman, G. J., et al. (2007), The TRMM Multisatellite Precipitation Analysis (TMPA): Quasi-global, multiyear, combined-sensor precipitation estimates at fine scales, *J. Hydrometeorol.*, *8*, 38–55, doi:10.1175/JHM560.1.

Ingleby, B., and M. Huddleston (2007), Quality control of ocean temperature and salinity profiles—Historical and real-time data, *J. Mar. Syst.*, *65*, 158–175, doi:10.1016/j.jmarsys.2005.11.019.

International Federation of Red Cross and Red Crescent Societies (2001), Situation report—India: Orissa cyclone. Appeal no. 28/99, *Situat. Rep. 17*, Geneva, Switzerland.

Jacob, S. D., and L. K. Shay (2003), The role of oceanic mesoscale features on the tropical cyclone-induced mixed layer response: A case study, *J. Phys. Oceanogr.*, *33*(4), 649–676, doi:10.1175/1520-0485(2003)33<649:TROOMF>2.0.CO;2.

Jacob, S. D., L. K. Shay, A. J. Mariano, and P. G. Black (2000), The 3D oceanic mixed layer response to Hurricane Gilbert, *J. Phys. Oceanogr.*, *30*(6), 1407–1429, doi:10.1175/1520-0485(2000)030<1407:TOMLRT>2.0.CO;2.

Jiang, X., Z. Zhong, and J. Jiang (2009), Upper ocean response of the South China Sea to Typhoon Krovanh (2003), *Dyn. Atmos. Oceans*, *47*(1–3), 165–175, doi:10.1016/j.dynatmoce.2008.09.005.

Kara, A. B., A. J. Wallcraft, and H. E. Hurlburt (2005a), A new solar radiation penetration scheme for use in ocean mixed layer studies: An application to the Black Sea using a fine-resolution Hybrid Coordinate Ocean Model (HYCOM), *J. Phys. Oceanogr.*, *35*(1), 13–32, doi:10.1175/JPO2677.1.

Kara, A. B., A. J. Wallcraft, and H. E. Hurlburt (2005b), Sea surface temperature sensitivity to water turbidity from simulations of turbid Black Sea using HYCOM, *J. Phys. Oceanogr.*, *35*, 33–54, doi:10.1175/JPO-2656.1.

Kikuchi, K., B. Wang, and H. Fudeyasu (2009), Genesis of tropical cyclone Nargis revealed by multiple satellite observations, *Geophys. Res. Lett.*, *36*, L06811, doi:10.1029/2009GL037296.

Kummerow, C., W. Barnes, T. Kozu, J. Shiue, and J. Simpson (1998), The Tropical Rainfall Measuring Mission (TRMM) sensor package, *J. Atmos. Oceanic Technol.*, *15*, 809–817, doi:10.1175/1520-0426(1998)015<0809:TTRMMT>2.0.CO;2.

Kummerow, C., et al. (2000), The status of the Tropical Rainfall Measuring Mission (TRMM) after two years in orbit, *J. Appl. Meteorol.*, *39*(12), 1965–1982, doi:10.1175/1520-0450(2001)040<1965:TSOTTR>2.0.CO;2.

Large, W. G., and S. Pond (1981), Open ocean momentum flux measurements in moderate to strong winds, *J. Phys. Oceanogr.*, *11*, 324–336, doi:10.1175/1520-0485(1981)011<0324:OOMFMI>2.0.CO;2.

Large, W. G., J. C. McWilliams, and S. C. Doney (1994), Ocean vertical mixing: A review and a model with a nonlocal boundary layer parameterization, *Rev. Geophys.*, *32*, 363–403, doi:10.1029/94RG01872.

Large, W. G., G. Danabasoglu, S. C. Doney, and J. C. McWilliams (1997), Sensitivity to surface forcing and boundary layer mixing in a global ocean model: Annual-mean climatology, *J. Phys. Oceanogr.*, *27*, 2418–2447, doi:10.1175/1520-0485(1997)027<2418:STSFAB>2.0.CO;2.

Latha, G., and E. P. Rama Rao (2007), Surge simulations for 1999 Orissa super cyclone using a finite element model, *Nat. Hazards*, *40*, 615–625, doi:10.1007/s11069-006-9012-2.

Ledwell, J. R., A. J. Watson, and C. S. Law (1993), Evidence for slow mixing across the pycnocline from an open-ocean tracer-release experiment, *Nature*, *364*, 701–703, doi:10.1038/364701a0.

Lin, I.-I., C.-H. Chen, I.-F. Pun, W. T. Liu, and C.-C. Wu (2009), Warm ocean anomaly, air sea fluxes, and the rapid intensification of tropical cyclone Nargis (2008), *Geophys. Res. Lett.*, *36*, L03817, doi:10.1029/2008GL035815.

Lukas, R., and E. Lindstrom (1991), The mixed layer of the western equatorial Pacific Ocean, *J. Geophys. Res.*, *96*, 3343–3357.

Macdonald, A. M., and C. Wunsch (1996), An estimate of global ocean circulation and heat fluxes, *Nature*, *382*, 436–439, doi:10.1038/382436a0.

Mahapatra, D. K., A. D. Rao, S. V. Babu, and C. Srinivas (2007), Influence of coast line on upper ocean's response to the tropical cyclone, *Geophys. Res. Lett.*, *34*, L17603, doi:10.1029/2007GL030410.

Mandal, M., U. C. Mohanty, P. Sinha, and M. M. Ali (2007), Impact of sea surface temperature in modulating movement and intensity of tropical cyclones, *Nat. Hazards*, *41*(3), 413–427, doi:10.1007/s11069-006-9051-8.

Masson, S., P. Delecluse, J. P. Boulanger, and C. Menkes (2002), A model study of the seasonal variability and formation mechanisms of the barrier layer in the eastern equatorial Indian Ocean, *J. Geophys. Res.*, *107*(C12), 8017, doi:10.1029/2001JC000832.

Meehl, G. A., W. M. Washington, W. D. Collins, J. M. Arblaster, A. Hu, L. E. Buja, W. G. Strand, and H. Teng (2005), How much more global warming and sea level rise?, *Science*, *307*, 1769–1772, doi:10.1126/science.1106663.

Meehl, G. A., J. M. Arblaster, J. T. Fasullo, A. Hu, and K. E. Trenberth (2011), Model-based evidence of deep-ocean heat uptake during surface-temperature hiatus periods, *Nat. Clim. Change*, *1*, 360–364, doi:10.1038/nclimate1229.

Murty, V. S. N., Y. V. B. Sarma, and D. P. Rao (1996), Variability of the oceanic boundary layer characteristics in the northern Bay of Bengal during MONTBLEX-90, *J. Earth Syst. Sci.*, *105*, 41–61.

NOAA (1979), Meteorological criteria for standard project hurricane and probable maximum hurricane wind fields, Gulf of Mexico and east coast of the United States, *Tech. Rep. NWS 23*, 320 pp., Washington, D. C.

Oey, L. Y., T. Ezer, D. P. Wang, X. Q. Yin, and S.-J. Fan (2007), Hurricane-induced motions and interaction with ocean currents, *Cont. Shelf Res.*, *27*(9), 1249–1263, doi:10.1016/j.csr.2007.01.008.

Powell, M. D., P. J. Vickery, and T. A. Reinhold (2003), Reduced drag coefficient for high wind speeds in tropical cyclones, *Nature*, *422*, 279–283, doi:10.1038/nature01481.

Prasad, T. G., and P. J. Hogan (2007), Upper-ocean response to Hurricane Ivan in a 1/25 degrees nested Gulf of Mexico HYCOM, *J. Geophys. Res.*, *112*, C04013, doi:10.1029/2006JC003695.

Price, J. F. (1981), Upper ocean response to a hurricane, *J. Phys. Oceanogr.*, *11*, 153–175, doi:10.1175/1520-0485(1981)011<0153:UORTAH>2.0.CO;2.

Rao, R. R., M. S. G. Kumar, M. Ravichandran, B. K. Samala, and N. Sreedevi (2006a), Observed mini-cold pool off the southern tip of India and its intrusion into the south central Bay of Bengal during summer monsoon season, *Geophys. Res. Lett.*, *33*, L06607, doi:10.1029/2005GL025382.

Rao, R. R., M. S. G. Kumar, M. Ravichandran, B. K. Samala, and G. Anitha (2006b), Observed intraseasonal variability of mini-cold pool off the southern tip of India and its intrusion into the south central Bay of Bengal during summer monsoon season, *Geophys. Res. Lett.*, *33*, L15606, doi:10.1029/2006GL026086.

Sanford, T. B., J. F. Price, J. B. Girton, and D. C. Webb (2007), Highly resolved observations and simulations of the ocean response to a hurricane, *Geophys. Res. Lett.*, *34*, L13604, doi:10.1029/2007GL029679.

Sengupta, D., B. Goddalehundi, and D. S. Anitha (2008), Cyclone-induced mixing does not cool SST in the post-monsoon north Bay of Bengal, *Atmos. Sci. Lett.*, *9*(1), 1–6, doi:10.1002/asl.162.

Shaji, C., C. Wang, G. R. Halliwell, and A. Wallcraft (2005), Simulation of tropical Pacific and Atlantic Oceans using a hybrid coordinate ocean model, *Ocean Modell.*, *9*(3), 253–282, doi:10.1016/j.ocemod.2004.07.003.

Shi, W., and M. Wang (2008), Three-dimensional observations from MODIS and CALIPSO for ocean responses to cyclone Nargis in the Gulf of Martaban, *Geophys. Res. Lett.*, *35*, L21603, doi:10.1029/2008GL035279.

Simmons, A., S. Uppala, D. Dee, and S. Kobayashi (2007), ERA-Interim: New ECMWF reanalysis products from 1989 onwards, *Newsl. 110*, 11 pp., Eur. Cent. for Medium-Range Weather Forecasts, Reading, U. K.

Siswanto, E., J. Ishizaka, A. Morimoto, K. Tanaka, K. Okamura, A. Kristijono, and T. Saino (2008), Ocean physical and biogeochemical responses to the passage of Typhoon Meari in the East China Sea observed from Argo float and multiplatform satellites, *Geophys. Res. Lett.*, *35*, L15604, doi:10.1029/2008GL035040.

Sprintall, J., and M. Tomczak (1992), Evidence of the barrier layer in the surface layer of the tropics, *J. Geophys. Res.*, *97*(C5), 7305–7316, doi:10.1029/92JC00407.

Sriver, R. L., and M. Huber (2007), Observational evidence for an ocean heat pump induced by tropical cyclones, *Nature*, *447*, 577–580, doi:10.1038/nature05785.

Sriver, R. L., M. Huber, and J. Nusbaumer (2008), Investigating tropical cyclone-climate feedbacks using the TRMM Microwave Imager and the Quick Scatterometer, *Geochem. Geophys. Geosyst.*, *9*, Q09V11, doi:10.1029/2007GC001842.

Subrahmanyam, B., V. S. N. Murty, R. J. Sharp, and J. J. O'Brien (2005), Air-sea coupling during the tropical cyclones in the Indian Ocean: A case study using satellite observations, *Pure Appl. Geophys.*, *162*, 1643–1672, doi:10.1007/s00024-005-2687-6.

Trenberth, K. E., and J. M. Caron (2001), Estimates of meridional atmosphere and ocean heat transports, *J. Clim.*, *14*, 3433–3443, doi:10.1175/1520-0442(2001)014<3433:EOMAAO>2.0.CO;2.

Tseng, Y. H., S. Jan, D. E. Dietrich, I.-I. Lin, Y. T. Chang, and T. Y. Tang (2010), Modeled oceanic response and sea surface cooling to Typhoon Kai-Tak, *Terr. Atmos. Oceanic Sci.*, *21*(1), 85–98, doi:10.3319/TAO.2009.06.08.02.

U.S. Navy (1999), Annual tropical cyclone report, U.S. Nav. Pac. Meteorol. and Oceanogr. Cent., Pearl Harbor, Hawaii. [Available at http://www.usno.navy.mil/NOOC/nmfc-ph/RSS/jtwc/atcr/1999atcr.pdf.]

Vinayachandran, P. N., V. S. N. Murty, and V. Ramesh Babu (2002), Observations of barrier layer formation in the Bay of Bengal during summer monsoon, *J. Geophys. Res.*, *107*(C12), 8018, doi:10.1029/2001JC000831.

Wada, A., H. Nino, and H. Nakano (2009), Roles of vertical turbulent mixing in the ocean response to Typhoon Rex (1998), *J. Oceanogr.*, *65*, 373–396, doi:10.1007/s10872-009-0034-8.

Wang, J.-W., W. Han, and R. L. Sriver (2012), Impact of tropical cyclones on the ocean heat budget in the Bay of Bengal during 1999: 2. Processes and interpretations, *J. Geophys. Res.*, *117*, C09021, doi:10.1029/2012JC008373.

Yin, X., Z. Wang, Y. G. Liu, and Y. Xu (2007), Ocean response to Typhoon Ketsana traveling over Northwest Pacific and a numerical model approach, *Geophys. Res. Lett.*, *34*, L21606, doi:10.1029/2007GL031477.

Yu, L., and M. J. McPhaden (2011), Ocean preconditioning of Cyclone Nargis in the Bay of Bengal: Interaction between Rossby waves, surface fresh waters, and sea surface temperatures, *J. Phys. Oceanogr.*, *41*(9), 1741–1755, doi:10.1175/2011JPO4437.1.

Yuan, D., W. Han, and D. Hu (2006), Surface Kuroshio path in the Luzon Strait area derived from satellite remote sensing data, *J. Geophys. Res.*, *111*, C11007, doi:10.1029/2005JC003412.

Zedler, S. E. (2009), Simulations of the ocean response to a hurricane: Nonlinear processes, *J. Phys. Oceanogr.*, *39*, 2618–2634, doi:10.1175/2009JPO4062.1.

Zedler, S. E., T. D. Dickey, S. C. Doney, J. F. Price, X. Yu, and G. L. Mellor (2002), Analyses and simulations of the upper ocean's response to Hurricane Felix at the Bermuda Testbed Mooring site: 13–23 August 1995, *J. Geophys. Res.*, *107*(C12), 3232, doi:10.1029/2001JC000969.

Zheng, Z., C. Ho, Q. Zheng, Y. Lo, N. Kuo, and G. Gopalakrishnan (2010), Effects of preexisting cyclonic eddies on upper ocean responses to category 5 typhoons in the western North Pacific, *J. Geophys. Res.*, *115*, C09013, doi:10.1029/2009JC005562.